
SGS-SLAM: SEMANTIC GAUSSIAN SPLATTING FOR NEURAL DENSE SLAM

A PREPRINT

Mingrui Li *

Department of Computer Science
Dalian University of Technology
2905450254@mail.dlut.edu.cn

Shuhong Liu *

Department of Information Science and Technology
The University of Tokyo
s-liu@isi.imi.i.u-tokyo.ac.jp

Heng Zhou

Department of Mechanical Engineering
Columbia University
henryzhou998@gmail.com

February 6, 2024

ABSTRACT

Semantic understanding plays a crucial role in Dense Simultaneous Localization and Mapping (SLAM), facilitating comprehensive scene interpretation. Recent advancements that integrate Gaussian Splatting into SLAM systems have demonstrated its effectiveness in generating high-quality renderings through the use of explicit 3D Gaussian representations. Building on this progress, we propose SGS-SLAM, the first semantic dense visual SLAM system grounded in 3D Gaussians, which provides precise 3D semantic segmentation alongside high-fidelity reconstructions. Specifically, we propose to employ multi-channel optimization during the mapping process, integrating appearance, geometric, and semantic constraints with key-frame optimization to enhance reconstruction quality. Extensive experiments demonstrate that SGS-SLAM delivers state-of-the-art performance in camera pose estimation, map reconstruction, and semantic segmentation, outperforming existing methods meanwhile preserving real-time rendering ability.

Keywords SLAM · 3D Reconstruction · 3D Semantic Segmentation

1 Introduction

Dense Visual Simultaneous Localization and Mapping (SLAM) is a crucial problem in the field of computer vision. It aims to reconstruct a dense 3D map in an unseen environment while simultaneously tracking the camera poses in a real-time manner. Traditional visual SLAM systems Davison et al. [2007], Newcombe et al. [2011], Salas-Moreno et al. [2013], Mur-Artal et al. [2015] have yielded notable achievements in the field of sparse reconstruction, but fall short in effectively representing dense reconstruction through point clouds or voxels. To extract dense geometric information for high-fidelity representation, learning-based SLAM methods Bloesch et al. [2018], Sucar et al. [2020] have gained wild attention. They demonstrate proficiency in generating decent global 3D maps meanwhile exhibiting robustness on noises and outliers. In addition, drawing inspiration from the advancements in the neural radiance field (NeRF) Mildenhall et al. [2021], NeRF-based SLAM approaches Sucar et al. [2021], Zhu et al. [2022], Kong et al. [2023], Zhang et al. [2023], Li et al. [2023a], Wang et al. [2023] have made further progress. They excel in producing accurate and high-fidelity global reconstruction by capturing dense photometric information through differentiable rendering.

*These authors contributed equally to this work

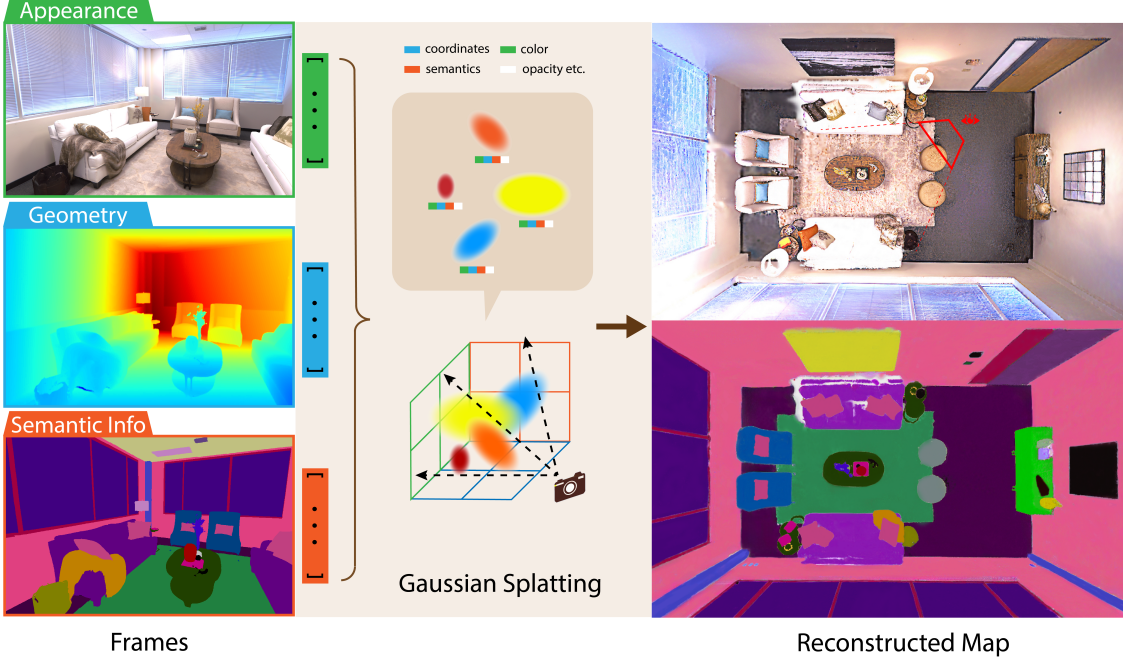


Figure 1: The illustration of the proposed SGS-SLAM. It employs multi-channel 2D inputs encompassing appearance, geometry, and semantic information, leveraging Gaussian Splatting and differentiable rendering for joint parameter optimization. SGS-SLAM delivers accurate 3D semantic mapping along with high-fidelity map reconstructions.

However, NeRF-based SLAM methods employ multi-layer perceptrons (MLPs) as the implicit neural representation of scenes, which introduces several challenging limitations. Primarily, MLP models struggle with over-smoothing issues at the edges of objects, leading to a lack of fine-grained details in the map. This challenge also brings difficulties on disentangling the representation of objects, making it non-trivial to segment, edit, and manipulate objects within the scene. Moreover, when applied to larger scenes, MLP models are prone to catastrophic forgetting. This means that incorporating new scenes can adversely affect the precision of previously learned models, thereby reducing overall performance. Additionally, NeRF-based methods are computationally inefficient. Since the entire scene is modeled through one or several MLPs, it necessitates extensive model tuning for adding or updating scenes.

In this context, as opposite to NeRF-based neural representation, our exploration shifts towards the volumetric representation based on the 3D Gaussian Radiance Field Kerbl et al. [2023]. This approach marks a significant shift and offers notable advantages in the scene representation.

Benefits from its rasterization of 3D primitives, Gaussian Splatting exhibits remarkably fast rendering speeds and allows direct gradient flow to each Gaussian's parameters. This results in an almost linear projection between the dense photometric loss and parameters during optimization, unlike the hierarchical pixel-sampling and indirect gradient flow through multiple non-linear layers seen in NeRF models. Moreover, the direct projection capability simplifies the addition of new parameters to the Gaussian field as separate channels, thereby enabling dynamic multi-channel rendering. Crucially, we integrate a semantic map into the 3D Gaussian field, essential for applications in robotics and mixed-reality, which allows for real-time switching between color, depth, and semantic color rendering. This stands in contrast to NeRF-based methods, which require the training of additional models and extra feature fusion for rendering when facing new input channels.

When compared with neural implicit semantic SLAM systems, such as DNS-SLAM Li et al. [2023a] and SNI-SLAM Zhu et al. [2023], our system demonstrates remarkable superiority in terms of rendering speed, scene precision, and segmentation accuracy. Leveraging these benefits, our method enable precise editing and manipulation of specific scene elements while preserving the high fidelity of the overall rendering. Furthermore, the utilization of explicit spatial and semantic information for identifying scene content can be instrumental in optimizing camera tracking. Particularly, we incorporate the adjustment based on geometric and semantic criteria for camera pose estimation, and utilize semantic constraints in the key-frames selection which relies on recognizing objects that have been previously observed in the trajectory.

Overall, our work presents several key contributions, summarized as follows:

- We introduce SGS-SLAM, a dense semantic SLAM system utilizing 3D Gaussians. SGS-SLAM employs an explicit volumetric representation, enabling swift and real-time camera tracking and scene mapping. More importantly, it utilizes 2D semantic maps to learn 3D semantic representations expressed by Gaussians. Compared with previous NeRF-based methods which offers over-smooth object edges, SGS-SLAM provides similar to ground-truth level segmentation precision.
- In SGS-SLAM, semantic maps provide additional supervision for optimizing parameters and selecting key frames. We employ a multi-channel parameter optimization strategy where appearance, geometric, and semantic signals collectively contribute to camera tracking and scene reconstruction. Furthermore, SGS-SLAM utilizes these diverse channels for the key-frame selection during the tracking phase, concentrating on actively recognizing objects seen earlier in the trajectory. This approach results in efficient and high-quality map reconstruction based on the chosen key frames.
- Utilizing semantic representation, SGS-SLAM provides a highly accurate disentangled object representation in 3D scenes, laying a solid foundation for downstream tasks such as scene editing and manipulation. SGS-SLAM facilitates the dynamic moving, rotating, or removal of objects in the map in real-time. This is achieved by identifying the semantic labels of the objects, while ensuring the rest of the scene remains unchanged and stable.

Extensive experiments are conducted on both synthetic and real-world scene benchmarks. These experiments compare our method against both NeRF-based implicit approaches and novel 3D-Gaussian-based methods, evaluating performance in mapping, tracking, and semantic segmentation.

2 Related Work

2.1 Semantic SLAM

Semantic information is of great importance for SLAM systems Mur-Artal et al. [2015], He et al. [2023], Whelan et al. [2015], Qin et al. [2018], which is a crucial requirement for applications in robotics and VR/AR fields. Real-time dense semantic SLAM systems Salas-Moreno et al. [2013], Bloesch et al. [2018], Rosinol et al. [2020] can integrate semantic information into 3D geometric representations. Traditional semantic SLAM systems rely on explicit 3D semantic expressions, such as voxel Hermans et al. [2014], point cloud Narita et al., and signed distance field Narita et al.. These methods have limitations in terms of reconstruction speed, high-fidelity model acquisition, and memory usage. Moreover, traditional methods cannot reasonably infer unknown areas.

2.2 Neural Implicit SLAM

Methods based on NeRF McCormac et al. [2018], which handle complex topological structures and differentiable scene representation methods, have garnered significant attention, leading to the development of neural implicit SLAM methods Li et al. [2023b], Chung et al. [2023]. iMAP Sucar et al. [2021] uses a single MLP for scene representation, which is limited in large-scale scenes. NICE-SLAM Zhu et al. [2022] uses pre-trained multiple MLPs for hierarchical scene representation. Co-SLAM Wang et al. [2023] combines pixel set-based keyframe tracking with One-blob encoding. Go-SLAM Zhang et al. [2023] uses Droid-SLAM front-end tracking and multi-resolution hash encoding Müller et al. [2022] for mapping while implementing loop closure detection and global optimization. However, these methods cannot utilize semantic information in maps. NIDS-SLAM Haghghi et al. [2023] leverages the mature front-end tracking of ORB-SLAM3 Campos et al. [2021] and Instant-NGP Müller et al. [2022] for mapping but does not optimize joint semantic features for 3D reconstruction. DNS-SLAM Li et al. [2023a] proposes a 2D semantic prior system that provides multi-view geometry constraints but does not optimize 3D reconstruction with semantic features. SNI-SLAM Zhu et al. [2023], a work parallel to ours, introduces semantic loss for geometric supervision but remains limited by the efficiency constraints of NeRF's volume rendering.

2.3 3D Gaussian Splatting-SLAM

The outstanding performance and fast rasterization capabilities of 3D Gaussian Splatting Kerbl et al. [2023] enable higher efficiency and accuracy on sparse pixel bases. However, existing 3DGS-based SLAM systems Yan et al. [2023], Keetha et al. [2023], Huang et al. [2023] lack traditional effective loop closure detection, limiting tracking accuracy and the ability to recognize semantic information in scenes. We fuse semantic features into geometry and appearance and integrate 3D semantic features during the tracking process for loop closure detection. This allows us to obtain more effective and higher-resolution scene segmentation results while maintaining real-time performance.

3 Method

3.1 Multi-Channel Gaussian Representation

The scene is represented using a gaussian influence function $f(\cdot)$ on the map. For simplicity, these Gaussians are isotropic, as proposed in Keetha et al. [2023]:

$$f^{3D}(x) = \sigma \exp\left(-\frac{\|x - \mu\|^2}{2r^2}\right) \quad (1)$$

Here, $\sigma \in [0, 1]$ indicates opacity, $\mu \in \mathbb{R}^3$ represents the center position, and r denotes the radius. Each Gaussian also carries RGB colors $c_i = [r_i \ b_i \ g_i]^T$.

In order to optimize the parameters of Gaussians to represent the scene, we need to render the Gaussians into 2D images in a differentiable manner. We use the render from Luiten et al. [2024], providing extended functionality of rendering depth in colors. It works by splatting 3D Gaussians into the image plane by approximating the projection of the integral of the influence function $f(\cdot)$ along the depth dimension in pixel coordinate. The center of the Gaussian μ , radius r , and depth d (in camera coordinates) is splatted using the standard point rendering formula:

$$\mu^{2D} = K \frac{E_t \mu}{d}, \quad r^{2D} = \frac{lr}{d}, \quad d = (E_t \mu)_z \quad (2)$$

where K is the camera intrinsic matrix, E_t is the extrinsic matrix capturing the rotation and translation of the camera at frame t , l is the focal length. The influence of all Gaussians on this pixel can be combined by sorting the Gaussians in depth order and performing front-to-back volume rendering using the Max volume rendering formula Max [1995]:

$$C_{pix} = \sum_{i=1}^n c_i f_{i,pix}^{2D} \prod_{j=1}^{i-1} (1 - f_{j,pix}^{2D}) \quad (3)$$

The pixel-level rendered color C_{pix} is the sum over the colors of each Gaussian c_i and weighted by the influence function $f_{i,pix}^{2D}$ (replace the 3D means and covariance matrices with the 2D splatted versions), multiplied by an occlusion term taking into account the effect of all Gaussians in front of the current Gaussian.

Similarly, the depth can be rendered as

$$D_{pix} = \sum_{i=1}^n d_i f_{i,pix}^{2D} \prod_{j=1}^{i-1} (1 - f_{j,pix}^{2D}) \quad (4)$$

where d_i denotes the depth of each Gaussian. By setting $d_i = 1$, we are able to calculate a silhouette, $Sil_{pix} = D_{pix}(d_i = 1)$, which assists in determining whether a pixel is visible in the current view. This aspect of visibility is essential for camera pose estimation, as it relies on the current reconstructed map. Additionally, it is also employed in map reconstruction, where new Gaussians are introduced in pixels lacking sufficient information.

While acquiring 3D semantic information is challenging and usually demands extensive manual labeling, 2D semantic label is a more accessible prior. In our approach, we leverage 2D semantic labels, which are often provided in datasets or can be easily obtained using state-of-the-art methods. We assign distinct channels to the parameters of Gaussians to denote their semantic labels and colors. During the rendering process, the 2D semantic map can be rendered from the reconstructed 3D scene as follows:

$$S_{pix} = \sum_{i=1}^n s_i f_{i,pix}^{2D} \prod_{j=1}^{i-1} (1 - f_{j,pix}^{2D}) \quad (5)$$

where $s_i = [r_i \ b_i \ g_i]^T$ denotes the semantic color associated with the Gaussian. This semantic color is optimized jointly with the appearance color and depth during the mapping process.

3.2 Tracking and Mapping

Like previous SLAM techniques, our method can be split into two processes: tracking and mapping. Tracking process estimates camera pose of each frame while keeping the scene parameters fixed. Mapping optimizes the scene representations based on the estimated camera pose. We break down steps into the following sections and explain in details.

3.2.1 Camera Pose Estimation

Given the first frame, the camera pose is set to identity and use as the reference coordinates for the following tracking and mapping procedure. While assessing the camera pose of an RGB-D view at a new timestep, the initial camera pose is determined by adding a displacement to the previous pose, assuming constant velocity, as $E_{t+1} = E_t + (E_t - E_{t-1})$. Following this, the current pose is iteratively refined by minimizing the tracking loss between the ground truth color (C_{pix}^{GT}), depth images (D_{pix}^{GT}), and semantic map (S_{pix}^{GT}) and their differentiably rendered views:

$$\mathcal{L}_{\text{tracking}} = \sum_{\text{pix}} (\text{Sil}_{\text{pix}} > T_S) (\lambda_D |D_{\text{pix}}^{GT} - D_{\text{pix}}| + \lambda_C |C_{\text{pix}}^{GT} - C_{\text{pix}}| + \lambda_S |S_{\text{pix}}^{GT} - S_{\text{pix}}|) \quad (6)$$

Here, only those rendered pixels with a sufficiently large silhouette are factored into the loss calculation. The threshold T_S is designed to make use of the map that has been previously optimized and has high certainty to be visible in the current camera view.

3.2.2 Key-frames Selection and Weighting

During the tracking phase of SLAM systems, key frames are identified and stored simultaneously. These key frames, providing different views of objects, are critical for mapping to refine 3D scene reconstruction. SGS-SLAM captures and stores key frames at constant time intervals. For mapping, key frames associated with the current frame are chosen based on geometric and semantic constraints. Specifically, we randomly select pixels from the current frame and extract their corresponding Gaussians G_{sample} in the 3D scene. These Gaussians, G_{sample} , are then projected onto the camera views of key frames as G_{proj} . The G_{proj} are evaluated based on the geometric overlap ratio:

$$\eta = \frac{1}{\sum G_{\text{proj}}} \sum_{n=i} \{G_i | 0 \leq \text{width}(G_i) \leq W, 0 \leq \text{height}(G_i) \leq H\} \quad (7)$$

It represents the proportion of Gaussians captured within the camera view of the key frames. W and H are the width and height of the camera view. The top K candidates are selected from this ranking. After the initial geometric-based selection, a second selection is conducted based on semantic criteria. We discard key frames whose semantic maps S_{pix} are identical to the current frame's semantic map, as indicated by a high mIoU score. This threshold intends to enhance map optimization from varying viewpoints, preferring views with low mIoU overlap. In addition, we compute an uncertainty score for each key frame, defined as $\mathcal{U}(t) = e^{-\tau t}$, with t representing the timestamp of the key frame and τ being a decay coefficient. This uncertainty score is used to weight the mapping loss $\mathcal{L}_{\text{mapping}}$. The intuition behind this is that key frames with a later timestamp index carry a higher uncertainty in reconstruction due to the accumulation of camera tracking errors along the trajectory.

3.2.3 Map Reconstruction

The scene is modeled using Gaussians across three distinct channels: (1) their mean coordinates represent the geometric information of the scene, (2) their appearance colors depict the scene's visual appearance, and (3) their semantic colors indicate the semantic labels of objects. These parameters across the channels are jointly optimized during the process of Gaussian densification and optimization, while the camera pose, ascertained from tracking, remains fixed.

Starting with the first frame, all pixels contribute to initializing the map. In the process of map reconstruction at a new timestep, new Gaussians are introduced to areas of the map that are either insufficiently dense or display new geometry in front of the previously estimated map. The addition of new Gaussians is regulated by applying a mask to the pixels where either (ii) the silhouette value Sil_{pix} falls below a certain threshold, signifying a high uncertainty in visibility, or (ii) $D_{\text{pix}}^{GT} < D_{\text{pix}}$, indicating that the ground-truth depth is much smaller than the estimated depth, and thus suggesting the presence of new geometrical features.

After densification, the parameters of the map are optimized by minimizing the mapping loss as:

$$\mathcal{L}_{\text{mapping}} = \mathcal{U} \sum_{\text{pix}} \lambda_D |D_{\text{pix}}^{GT} - D_{\text{pix}}| + \lambda_C \mathcal{L}_C + \lambda_S \mathcal{L}_S \quad (8)$$

where \mathcal{L}_C and \mathcal{L}_S are weighted SSIM loss Kerbl et al. [2023] with respect to appearance image and semantic image:

$$\mathcal{L}(I_{\text{pix}}) = \sum_{\text{pix}} \alpha |I_{\text{pix}}^{GT} - I_{\text{pix}}| + (1 - \alpha) (1 - \text{ssim}(I_{\text{pix}}^{GT}, I_{\text{pix}})) \quad (9)$$

Here, λ_D , λ_C , λ_S , and α are predefined hyperparameters, and \mathcal{U} is the uncertainty score defined in section 3.2.2.

Compared to current NeRF-based methods, which demand complex model architectures and feature fusion strategies for the optimization of geometric, appearance, and semantic features, Gaussian representation offers a notable advantage. The complexity in NeRF-based methods primarily arises from their implicit representation of scenes, where each feature is modeled by a MLP separately, often leading to limited performance. In contrast, Gaussian representation, with its explicit definition of scene parameters, facilitates direct gradient flow to each parameter. This enables the joint optimization of parameters across different channels, remarkably enhancing the efficiency and effectiveness of both mapping and segmentation processes.

4 Experiment

4.1 Experimental Setup

Datasets We evaluate our method on both synthetic and real-world datasets. To compare with other neural implicit SLAM methods, we evaluate on 8 synthetic scenes from Replica dataset Straub et al. [2019] and real-world scenes from ScanNet Dai et al. [2017a]. The ground-truth camera pose and semantic map of Replica are offered from simulation, and ground-truth camera pose of ScanNet is generated by BundleFusion Dai et al. [2017b].

Metrics We use PSNR, Depth-L1 (on 2D depth map), SSIM, and LPIPS to evaluate the reconstruction quality. For the evaluation of camera pose, we adopt the average absolute trajectory error (ATE RMSE). For semantic segmentation, we calculate mIoU score.

Baselines We compare the tracking and mapping with state-of-the-art methods iMap Sucar et al. [2021], Vox-Fusion Yang et al. [2022], NICE-SLAM Zhu et al. [2022], Co-SLAM Wang et al. [2023], ESLAM Johari et al. [2023], and SplaTAM Keetha et al. [2023]. For semantic segmentation accuracy, we compare with NIDS-SLAM Haghghi et al. [2023], DNS-SLAM Li et al. [2023a], and SNI-SLAM Zhu et al. [2023].

4.2 Experimental Results

We show quantitative measures of reconstruction quality using the Replica dataset in Table 1. Our method demonstrates state-of-the-art performance. When compared to other baseline methods, our approach attains notably superior outcomes, outperforming them by a margin of 10dB in PSNR.

In Figure 2, we present the reconstruction results of three chosen scenes, where regions of interest are accentuated with boxes in various colors. Our method exhibits high-fidelity reconstruction outcomes. Specifically, for small, intricately textured objects like a clock, socket, books on a tea table, and a lamp, our approach shows remarkable accuracy over NeRF-based methods. This is because Gaussians are capable of representing objects with complex textures and surfaces. Furthermore, NeRF-based methods often struggle with the over-smoothing issue, resulting in blurred edges on objects. In contrast, by utilizing an explicit Gaussian representation, SGS-SLAM precisely captures objects with clear edges, irrespective of their sizes. Compared with SplaTAM, which is also a Gaussian-based model, our approach utilizes semantic information for discerning object categories, recognizing visual appearance to determine texture, and applies geometric constraints to preserve accurate shapes. This combination enables our method to achieve thorough modeling of both objects and their surrounding environment. The combination of these constraints allows SGS-SLAM to capture fine-grained details of objects, offering high-fidelity and accurate reconstruction.

Table 2 displays the tracking evaluation results on the Replica dataset. Our method excels in achieving the highest level of depth L1 loss (cm) and minimal ATE error, surpassing baseline methods by 70% in terms of depth loss and 34% in terms of ATE RMSE (cm). This exceptional performance can be attributed to our precise scene reconstruction, which provides finely-detailed rendering results. The high-quality rendering, in turn, contributes to accurate camera pose estimation based on the established map by preventing incorrect geometric reconstruction, which could otherwise result in inaccurate tracking outcomes. Additionally, utilizing features from different channels of Gaussians, such as



Figure 2: Qualitative comparison of our method and the baselines for reconstruction across three scenes from the Replica Dataset, with key details accentuated using colorful boxes. The results demonstrate that our method delivers more high-fidelity and robust reconstructions, particularly by capturing more detailed features of the objects in the scene.

geometry, appearance, and semantic information, provides multiple levels of supervision, resulting in a more robust and accurate tracking capability.

4.3 3D Semantic Segmentation

SGS-SLAM is the first Gaussian-based SLAM system that accomplishes simultaneous localization, reconstruction, and segmentation in a single framework. Table 3 shows a quantitative evaluation of our method in comparison to other neural semantic SLAM approaches. It's worth noting that we only show four scenes because previous NeRF-based semantic models only reported results on these scenes. In comparison to these previous methods, SGS-SLAM demonstrates state-of-the-art performance, outperforming the initial baseline by more than 10%. Substantial enhancement highlights the crucial advantage of explicit Gaussian representation over implicit NeRF representation. Gaussians can precisely isolate object boundaries, resulting in highly accurate 3D scene segmentation. In contrast, NeRF-based methods often struggle to recognize individual objects and typically require complex multi-level model designs and extensive feature fusion. Our approach offers an unparalleled ability to identify 3D objects in decomposed representations, which can serve as 3D priors for tracking and mapping in future time steps, and is well-suited for further downstream tasks.

Methods	Metrics	Average	Room0	Room1	Room2	Office0	Office1	Office2	Office3	Office4
NICE-SLAM	PSNR↑	24.42	22.12	22.47	24.52	29.07	30.34	19.66	22.23	24.94
	SSIM↑	0.809	0.689	0.757	0.814	0.874	0.886	0.797	0.801	0.856
	LPIPS↓	0.233	0.330	0.271	0.208	0.229	0.181	0.235	0.209	0.198
Vox-Fusion	PSNR↑	24.41	22.39	22.36	23.92	27.79	29.83	20.33	23.47	25.21
	SSIM↑	0.801	0.683	0.751	0.798	0.857	0.876	0.794	0.803	0.847
	LPIPS↓	0.236	0.303	0.269	0.234	0.241	0.184	0.243	0.213	0.199
Co-SLAM	PSNR↑	30.24	27.27	28.45	29.06	34.14	34.87	28.43	28.76	30.91
	SSIM↑	0.939	0.910	0.909	0.932	0.961	0.969	0.938	0.941	0.955
	LPIPS↓	0.252	0.324	0.294	0.266	0.209	0.196	0.258	0.229	0.236
ESLAM	PSNR↑	29.08	25.32	27.77	29.08	33.71	30.20	28.09	28.77	29.71
	SSIM↑	0.929	0.875	0.902	0.932	0.960	0.923	0.943	0.948	0.945
	LPIPS↓	0.336	0.313	0.298	0.248	0.184	0.228	0.241	0.196	0.204
Ours	PSNR↑	34.15	32.50	34.25	35.10	38.54	39.10	31.90	30.05	31.75
	SSIM↑	0.973	0.976	0.978	0.982	0.984	0.982	0.965	0.966	0.949
	LPIPS↓	0.096	0.070	0.094	0.070	0.086	0.087	0.101	0.115	0.148

Table 1: Quantitative comparison of our method and the baselines in training view rendering on the Replica dataset. Our method demonstrates SOTA performances on all three metrics.

Methods	Depth L1↓ [cm]	ATE Mean↓ [cm]	ATE RMSE↓ [cm]	Param. ↓ [Mb]	Track. FPS↑ Unit	Map. FPS↑ Unit	SLAM FPS↑ Unit
iMAP	4.645	3.118	4.153	1.04	9.92	2.23	1.82
NICE-SLAM	1.903	1.795	2.503	12.02	13.70	0.20	0.20
Co-SLAM	1.513	0.935	1.059	0.26	17.24	10.20	6.41
ESLAM	1.180	0.520	0.630	6.79	18.11	3.62	3.02
Ours	0.356	0.327	0.412	0.01	5.27	3.52	2.11

Table 2: Quantitative comparison in terms of Depth, ATE, memory usage, and FPS between our method and the baselines on the Replica dataset. The values of baselines are retrieved from Zhu et al. [2023]. Our method remarkably outperforms the baselines at Depth and ATE evaluations, and performs fairly on FPS metrics. Note that for parameter size, we only count the parameters of the model.

4.3.1 Key Frame Optimization

In real-world datasets, tracking errors tend to accumulate along a trajectory, making pose estimations at later timestamps less reliable. Such inaccuracies can compromise the quality of map reconstructions, negatively impacting the accuracy of a previously well-established scene. A case in point is scene0000 from the ScanNet dataset, where objects such as bike and guitar are revisited at early and late stages in the trajectory. Key frames from later in the sequence, influenced by inaccurate camera poses, can disrupt the previously accurate reconstructions of these objects. Figure 3 illustrates the novel-view evaluation for scene0000. In comparison to SplaTAM, depicted in the upper row, our method delivers more accurate reconstruction outcomes. The bike, garbage bin, and guitar are accurately rendered, meanwhile details are preserved. Our method facilitates the selection of key frames base on geometric and semantic constraints, incorporating an uncertainty weighting during the optimization of selected key frames. This strategy demonstrate its effectiveness in map optimization from different views meanwhile preventing the unreliable key frame with high uncertainty to significantly altering the earlier accurately reconstructed map.

4.3.2 Scene Manipulation

The obtained semantic mask within the 3D scene has a range of applications for subsequent tasks. As an illustrative example, we demonstrate an straightforward but efficient Gaussian editing method, which is crucial for enabling scene manipulation for robotics or mixed reality applications. Specifically, the Gaussians generated during mapping, defined by equation 1, can be further utilized as:

$$f_{\text{edit}}^{\text{3D}}(G, \tilde{y}) = \mu(G, \tilde{y}) \cdot \Phi_T(f^{\text{3D}}(G), \tilde{y}) \quad (10)$$

Methods	Avg. mIoU \uparrow	Room0	Room1	Room2	Office0
NIDS-SLAM	82.37	82.45	84.08	76.99	85.94
DNS-SLAM	84.77	88.32	84.90	81.20	84.66
SNI-SLAM	87.41	88.42	87.43	86.16	87.63
Ours	92.72	92.95	92.91	92.10	92.90

Table 3: Quantitative comparison of our method against existing semantic NeRF-based SLAM methods on the Replica dataset. The baselines are limited to four scenes as their results are reported only for these. For each scene, we compute the average mIoU score by comparing the rendered and the ground-truth 2D semantic image in the training view. Our method significantly outperforms the NeRF-based approaches, achieving mIoU scores over 90%.



Figure 3: The selected novel view evaluation of scene0000 from the ScanNet dataset. The rendered views display the reconstructed bike and guitar captured within the trajectory. Our method outperforms SplaTAM by a large margin primarily due to the integration of key-frame optimization.

where the edited Gaussians, $f_{\text{edit}}^{\text{3D}}$, are influenced by the visibility function μ , transition function Φ_T , and the Gaussian's semantic label \tilde{y} . The visibility function μ determines if the Gaussians should be retained (1) or removed (0) based on \tilde{y} . The transition function Φ_T applies a transformation to the Gaussian's coordinates on selected \tilde{y} , enabling spatial manipulation.

Utilizing the decoupled scene representation, in contrast to NeRF-based approaches that demand fine-tuning of the entire network, we have the ability to choose specific objects within the scene by referencing their semantic mask while keeping the remainder of the well-trained, irrelevant environment fixed. As shown in Figure 4, for object removal, we can directly erase the Gaussians associated with the editing target, such as removing the table while preserving all the items on it. In addition, we can group objects by selecting their semantic masks and apply translation and rotation, such as moving and rotating both the table and the above objects to a different place. This editing capability requires no training or fine-tuning, making it readily available for downstream applications.

5 Conclusion

We presented SGS-SLAM, the first semantic dense visual SLAM system based on the 3D Gaussian representation. We propose to leverage multi-channel parameter optimization where appearance, geometric, and semantic constraints are combined to enforce high-accurate 3D semantic segmentation, and high-fidelity dense map reconstruction meanwhile effectively produce a robust camera pose estimation. SGS-SLAM takes the advantages of optimal key-frame optimization, resulting in reliable reconstruction quality. Extensive experiments show that our method provides state-of-the-art tracking and mapping results, meanwhile maintain rapid rendering speeds. Furthermore, the high-quality reconstruction

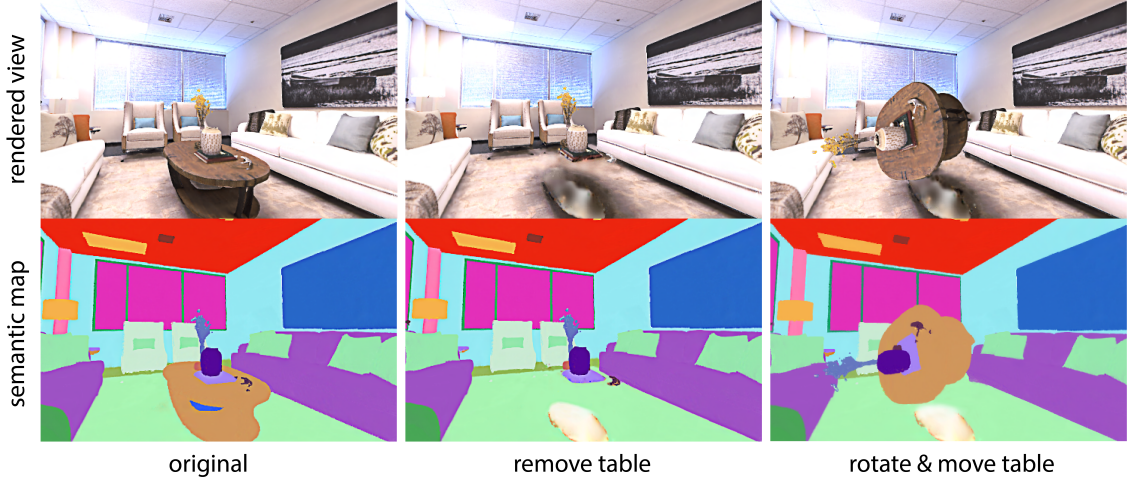


Figure 4: The case study on scene manipulation in room0 of the Replica dataset. We show the capabilities for object removal and transformation by specifying semantic labels. SGS-SLAM allows manipulation of either individual objects or a group of items, as illustrated by actions that include the removal of a table, as well as moving and rotating the table together with all objects on it.

of scenes and precise 3D semantic labeling generated by our system establish a strong foundation for the downstream tasks such as scene editing, offers solid prior for the robotics or AR/VR applications.

References

Andrew J Davison, Ian D Reid, Nicholas D Molton, and Olivier Stasse. Monoslam: Real-time single camera slam. *IEEE transactions on pattern analysis and machine intelligence*, 29(6):1052–1067, 2007.

Richard A Newcombe, Steven J Lovegrove, and Andrew J Davison. Dtam: Dense tracking and mapping in real-time. In *2011 international conference on computer vision*, pages 2320–2327. IEEE, 2011.

Renato F Salas-Moreno, Richard A Newcombe, Hauke Strasdat, Paul HJ Kelly, and Andrew J Davison. Slam++: Simultaneous localisation and mapping at the level of objects. In *Proceedings of the IEEE conference on computer vision and pattern recognition*, pages 1352–1359, 2013.

Raul Mur-Artal, Jose Maria Martinez Montiel, and Juan D Tardos. Orb-slam: a versatile and accurate monocular slam system. *IEEE transactions on robotics*, 31(5):1147–1163, 2015.

Michael Bloesch, Jan Czarnowski, Ronald Clark, Stefan Leutenegger, and Andrew J Davison. Codeslam—learning a compact, optimisable representation for dense visual slam. In *Proceedings of the IEEE conference on computer vision and pattern recognition*, pages 2560–2568, 2018.

Edgar Sucar, Kentaro Wada, and Andrew Davison. Nodeslam: Neural object descriptors for multi-view shape reconstruction. In *2020 International Conference on 3D Vision (3DV)*, pages 949–958. IEEE, 2020.

Ben Mildenhall, Pratul P Srinivasan, Matthew Tancik, Jonathan T Barron, Ravi Ramamoorthi, and Ren Ng. Nerf: Representing scenes as neural radiance fields for view synthesis. *Communications of the ACM*, 65(1):99–106, 2021.

Edgar Sucar, Shikun Liu, Joseph Ortiz, and Andrew J Davison. imap: Implicit mapping and positioning in real-time. In *Proceedings of the IEEE/CVF International Conference on Computer Vision*, pages 6229–6238, 2021.

Zihan Zhu, Songyou Peng, Viktor Larsson, Weiwei Xu, Hujun Bao, Zhaopeng Cui, Martin R Oswald, and Marc Pollefeys. Nice-slam: Neural implicit scalable encoding for slam. In *Proceedings of the IEEE/CVF Conference on Computer Vision and Pattern Recognition*, pages 12786–12796, 2022.

Xin Kong, Shikun Liu, Marwan Taher, and Andrew J Davison. vmap: Vectorised object mapping for neural field slam. In *Proceedings of the IEEE/CVF Conference on Computer Vision and Pattern Recognition*, pages 952–961, 2023.

Youmin Zhang, Fabio Tosi, Stefano Mattoccia, and Matteo Poggi. Go-slam: Global optimization for consistent 3d instant reconstruction. In *Proceedings of the IEEE/CVF International Conference on Computer Vision*, pages 3727–3737, 2023.

Kunyi Li, Michael Niemeyer, Nassir Navab, and Federico Tombari. Dns slam: Dense neural semantic-informed slam. *arXiv preprint arXiv:2312.00204*, 2023a.

Hengyi Wang, Jingwen Wang, and Lourdes Agapito. Co-slam: Joint coordinate and sparse parametric encodings for neural real-time slam. In *Proceedings of the IEEE/CVF Conference on Computer Vision and Pattern Recognition*, pages 13293–13302, 2023.

Bernhard Kerbl, Georgios Kopanas, Thomas Leimkühler, and George Drettakis. 3d gaussian splatting for real-time radiance field rendering. *ACM Transactions on Graphics*, 42(4), 2023.

Siting Zhu, Guangming Wang, Hermann Blum, Jiuming Liu, Liang Song, Marc Pollefeys, and Hesheng Wang. Sni-slam: Semantic neural implicit slam. *arXiv preprint arXiv:2311.11016*, 2023.

Jiaming He, Mingrui Li, Yangyang Wang, and Hongyu Wang. Ovd-slam: An online visual slam for dynamic environments. *IEEE Sensors Journal*, 2023.

Thomas Whelan, Stefan Leutenegger, Renato Salas-Moreno, Ben Glocker, and Andrew Davison. Elasticfusion: Dense slam without a pose graph. *Robotics: Science and Systems*, 2015.

Tong Qin, Peiliang Li, and Shaojie Shen. Vins-mono: A robust and versatile monocular visual-inertial state estimator. *IEEE Transactions on Robotics*, 34(4):1004–1020, 2018.

Antoni Rosinol, Marcus Abate, Yun Chang, and Luca Carlone. Kimera: an open-source library for real-time metric-semantic localization and mapping. In *2020 IEEE International Conference on Robotics and Automation (ICRA)*, pages 1689–1696. IEEE, 2020.

Alexander Hermans, Georgios Floros, and Bastian Leibe. Dense 3d semantic mapping of indoor scenes from rgb-d images. In *2014 IEEE International Conference on Robotics and Automation (ICRA)*, pages 2631–2638. IEEE, 2014.

Gaku Narita, Takashi Seno, Tomoya Ishikawa, and Yohsuke Kaji. Panopticfusion: Online volumetric semantic mapping at the level of stuff and things. in *2019 ieee. In RSJ International Conference on Intelligent Robots and Systems (IROS)*, pages 4205–4212.

John McCormac, Ronald Clark, Michael Bloesch, Andrew Davison, and Stefan Leutenegger. Fusion++: Volumetric object-level slam. In *2018 international conference on 3D vision (3DV)*, pages 32–41. IEEE, 2018.

Mingrui Li, Jiaming He, Yangyang Wang, and Hongyu Wang. End-to-end rgb-d slam with multi-mlps dense neural implicit representations. *IEEE Robotics and Automation Letters*, 2023b.

Chi-Ming Chung, Yang-Che Tseng, Ya-Ching Hsu, Xiang-Qian Shi, Yun-Hung Hua, Jia-Fong Yeh, Wen-Chin Chen, Yi-Ting Chen, and Winston H Hsu. Orbeez-slam: A real-time monocular visual slam with orb features and nerf-realized mapping. In *2023 IEEE International Conference on Robotics and Automation (ICRA)*, pages 9400–9406. IEEE, 2023.

Thomas Müller, Alex Evans, Christoph Schied, and Alexander Keller. Instant neural graphics primitives with a multiresolution hash encoding. *ACM Transactions on Graphics (ToG)*, 41(4):1–15, 2022.

Yasaman Haghghi, Suryansh Kumar, Jean Philippe Thiran, and Luc Van Gool. Neural implicit dense semantic slam. *arXiv preprint arXiv:2304.14560*, 2023.

Carlos Campos, Richard Elvira, Juan J Gómez Rodríguez, José MM Montiel, and Juan D Tardós. Orb-slam3: An accurate open-source library for visual, visual-inertial, and multimap slam. *IEEE Transactions on Robotics*, 37(6):1874–1890, 2021.

Chi Yan, Delin Qu, Dong Wang, Dan Xu, Zhigang Wang, Bin Zhao, and Xuelong Li. Gs-slam: Dense visual slam with 3d gaussian splatting. *arXiv preprint arXiv:2311.11700*, 2023.

Nikhil Keetha, Jay Karhade, Krishna Murthy Jatavallabhula, Gengshan Yang, Sebastian Scherer, Deva Ramanan, and Jonathon Luiten. Splatam: Splat, track & map 3d gaussians for dense rgb-d slam. *arXiv preprint arXiv:2312.02126*, 2023.

Huajian Huang, Longwei Li, Hui Cheng, and Sai-Kit Yeung. Photo-slam: Real-time simultaneous localization and photorealistic mapping for monocular, stereo, and rgb-d cameras. *arXiv preprint arXiv:2311.16728*, 2023.

Jonathon Luiten, Georgios Kopanas, Bastian Leibe, and Deva Ramanan. Dynamic 3d gaussians: Tracking by persistent dynamic view synthesis. In *3DV*, 2024.

Nelson Max. Optical models for direct volume rendering. *IEEE Transactions on Visualization and Computer Graphics*, 1(2):99–108, 1995.

Julian Straub, Thomas Whelan, Lingni Ma, Yufan Chen, Erik Wijmans, Simon Green, Jakob J Engel, Raul Mur-Artal, Carl Ren, Shobhit Verma, et al. The replica dataset: A digital replica of indoor spaces. *arXiv preprint arXiv:1906.05797*, 2019.

Angela Dai, Angel X Chang, Manolis Savva, Maciej Halber, Thomas Funkhouser, and Matthias Nießner. Scannet: Richly-annotated 3d reconstructions of indoor scenes. In *Proceedings of the IEEE conference on computer vision and pattern recognition*, pages 5828–5839, 2017a.

Angela Dai, Matthias Nießner, Michael Zollhöfer, Shahram Izadi, and Christian Theobalt. Bundlefusion: Real-time globally consistent 3d reconstruction using on-the-fly surface reintegration. *ACM Transactions on Graphics (ToG)*, 36(4):1, 2017b.

Xingrui Yang, Hai Li, Hongjia Zhai, Yuhang Ming, Yuqian Liu, and Guofeng Zhang. Vox-fusion: Dense tracking and mapping with voxel-based neural implicit representation. In *2022 IEEE International Symposium on Mixed and Augmented Reality (ISMAR)*, pages 499–507. IEEE, 2022.

Mohammad Mahdi Johari, Camilla Carta, and François Fleuret. Eslam: Efficient dense slam system based on hybrid representation of signed distance fields. In *Proceedings of the IEEE/CVF Conference on Computer Vision and Pattern Recognition*, pages 17408–17419, 2023.